An Orbit Robust Control Based on Linear Matrix Inequalities

D. Prieto* and B. Bona*

*Department of Control and Computer Engineering, Politecnico di Torino, Corso Duca degli Abruzzi, 24 Turin 10129, Italy
(Tel: +39-011-5645734; Fax: +39-011-5645909; Email: luis.prieto@polito.it)

Abstract: This paper considers the problem of satellite's orbit control and a solution based in Linear Matrix Inequalities (LMI) is proposed for the case of Low Earth Orbiters (LEO). In particular, the modelling procedure and the algorithm for control law synthesis are tested using as study case the European Gravity Field and Ocean Circulation Explorer satellite (GOCE), to be launched by the European Space Agency (ESA) in the year 2006. The scientific objective of this space mission is the recovering of the Earth gravity field with high accuracy (less than $10\mu m/s^2$) and spatial resolution (better than $100km$). In order to meet these scientific requirements, the orbit control must guarantee stringent specifications in terms of environmental disturbances attenuation (atmospheric drag forces) even in presence of high levels of model uncertainty.

Keywords: Orbit control, Low Earth Orbiter (LEO), Linear matrix inequality (LMI), H_∞ control, Multi Input Multi Output (MIMO) non linear control.

1. Introduction and background

1.1. The orbit control problem in LEO

The main purpose of an orbit control system (OCS) is to guarantee the tracking of a predefined orbit despite the effects of exogenous disturbances (such as gravitational perturbations, atmospheric drag, solar radiation pressure), actuators and measurement noise and uncertainty in the mathematical model definition. This paper offers a general framework for the formulation and solution of the OCS for the most common type of spacecraft rounding the Earth: the satellites launched into near circular orbits with altitudes between $250km$ and $1500km$. The most frequent use of Low Earth Orbiters is in remote sensing missions, where the higher spatial resolution at lower altitudes is used for developing complex measurements in a variety of spectral bands associated with specific scientific and technological missions.

1.2. The GOCE mission

The European mission Gravity Field and Steady-State Ocean Circulation Explorer(GOCE) is dedicated to the extremely high accurate measuring of the Earth's gravity field (less than $10\mu m/s^2$) and modelling the geoid (accuracy of $1-2cm$) at a spatial resolution better than $100km$ [1]. The mission will be developed with the following main elements: a single rigid octagonal spacecraft of approximately $5m$ long and $1m$ in diameter with fixed solar wings and no moving parts (Fig. 2(a)), a 12-channel GPS receiver

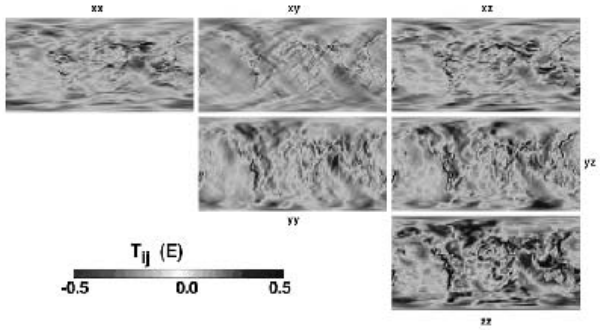

Fig. 1. Objectives of the GOCE mission: global model of the Earth's gravity field and geoid (courtesy ESA)

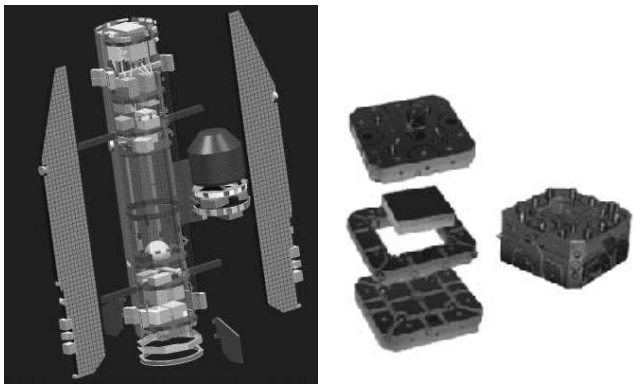

(a) CAD view of spacecraft (b) Prototype of accelerometer

Fig. 2. Elements of the GOCE mission (courtesy ESA)

with geodetic quality (for implementing Precise Orbit Determination, POD), a laser retroreflector enabling tracking by ground-based lasers and an ensemble of 3 pairs of three-axial electrostatic accelerometers (gravity gradiometer), each one containing a $320g$ proof mass electrostatically suspended and mechanically isolate from the spacecraft's main body through a specially engineered 'cage' (Fig. 2(b)). The specific role of the OCS for GOCE can be defined as an advanced drag compensation system that keeps the six proof masses in near 'free fall motion' and maintains the average orbital altitude at about $250km$. To develop these tasks, the forces that maintain each proof mass at the center of the cage are measured and the deviation from the nominal position within the allowed clearance band is used by the OCS for commanding the orbit propulsion subsystem (pair of Ion propulsion thrusters), that compensates the non-gravitational disturbance forces. The GOCE is thus forced to chase the proof mass, actively shielding it from the non-gravitational forces, the largest of which is the atmospheric drag. The net effect is that combining the differential accelerations, it is possible to derive the gravity gradient components.

1.3. Main contributions and paper organization

In this paper is proposed an approach for the orbit model definition based on spherical coordinates instead of the clas-

sical cartesian framework [2], [3], [4]. This allows to deduce a space state model (sections 2 and 3) characterized for an explicit relation with some classical orbit parameters (semi-major axis, eccentricity, epoch of passage from the perigee) and hence, offers more flexibility and clearness for analyzing the effects of any linear or non linear approximation. Also, the formulation of the OCS into a robust control framework [5], [6], allows to approximate the orbital dynamics through a relatively low complexity model, that includes a mathematical description of the system's uncertainty (section 4) as well as a detail analysis of the exogenous disturbances (section 5). The application of modern $H\infty$ synthesis theories for Singular Value (SV) shaping (section 6) offers optimal results for tracking, disturbance rejection and robustness aspects (section 7) when compared to space-feedback methods [3] or to frequency-weighted LQG (H_2) synthesis [7]. In addition, the Linear Matrix Inequality approach offers a more flexible frame for $H\infty$ synthesis than state-space design techniques [8] because its applicable in transfer functions (from controls to controlled outputs and from disturbances to measured outputs) with invariant zeros on the imaginary axis (as in the present case). Also, it requires only two main assumptions in the augmented model [8]: one, the pairs A, B_2 and A, C_2 shall be stabilizable and detectable respectively (the minimum for plant stabilization by dynamic output feedback); second, D_{22} shall be equal to zero (proper plant).

2. Reference frames

For establishing the mathematical model of LEO's motion, it is necessary to define a set of coordinate systems that allows a correct and easy integration of all the phenomena involved:

2.1. Inertial reference frame (IRF)

For practical purposes, a geocentric coordinate system is a suitable IRF due to the almost circular and unaccelerated motion of the Earth around the sun (orbit period $>$ 365 days) [9]. Based on this consideration, it is defined an IRF with origin at the Earth's Center of Mass (CoM); the Z_j axis, is the axis of Earth's rotation that intersects the celestial sphere at the north celestial pole; the X_j axis coincides with the vernal equinox vector (at the epoch January 1, 2000); the Y_j axis completes the right-handed orthogonal coordinate system.

2.2. Local Orbit Reference Frame (LORF)

It is a non-inertial reference frame used for describing the drag forces that perturbate the LEO. The origin is placed in the CoM of the spacecraft; the X_L axis is parallel to the instantaneous orbital velocity vector ($\boldsymbol{v}$); the Y_L axis is parallel to the instantaneous direction of the orbit angular momentum ($\boldsymbol{h} = \boldsymbol{r} \times \boldsymbol{v}$); the Z_L axis completes the right-handed orthogonal coordinate system.

2.3. Natural Orbit Reference Frame (NORF)

It is a non-inertial reference frame, suitable for the deduction of a space state model that describes the physical phenomena in terms of orbit plane (nominal case) and out-of-plane dimensions. The origin is placed in the Earth's Center of Mass; the X_N axis points toward the perigee in the orbit plane; the Z_N axis is parallel to the instantaneous direction of the orbit angular momentum ($\boldsymbol{h} = \boldsymbol{r} \times \boldsymbol{v}$); the Y_N axis completes the right-handed orthogonal coordinate system.

2.4. Transformation between reference frames

The transformation from NORF to IRF is provided through the following transformation matrix:

$$\begin{bmatrix} \boldsymbol{X_j} \\ \boldsymbol{Y_j} \\ \boldsymbol{Z_j} \end{bmatrix} = \Big[\boldsymbol{R_z(-\Omega) R_x(-i) R_z(-\omega)} \Big] \begin{bmatrix} \boldsymbol{X_N} \\ \boldsymbol{Y_N} \\ \boldsymbol{Z_N} \end{bmatrix} \tag{1}$$

where, $R_A(B)$ is a transformation matrix that represents a rotation about an axis A by the angle B. Specifically in (1), the Z_N axis is first rotate clockwise by the argument of the perigee (ω), aligning the original X_N axis with the line of nodes. Then, the X axis of this new coordinate system is rotated clockwise by the inclination angle (i), aligning the orbit plane with the Earth's Equatorial plane. Finally, the Z axis of this new coordinate system is rotated clockwise by the right ascension of the ascending node (Ω). The transformation from LORF to IRF is provided through the following rotation matrix:

$$\begin{bmatrix} \boldsymbol{X_j} \\ \boldsymbol{Y_j} \\ \boldsymbol{Z_j} \end{bmatrix} = \begin{bmatrix} \frac{\boldsymbol{v}}{\|\boldsymbol{v}\|} & \frac{\boldsymbol{v}\times\boldsymbol{r}}{\|\boldsymbol{v}\times\boldsymbol{r}\|} & \frac{\boldsymbol{v}\times\boldsymbol{r}\times\boldsymbol{v}}{\|\boldsymbol{v}\times\boldsymbol{r}\times\boldsymbol{v}\|} \end{bmatrix} \begin{bmatrix} \boldsymbol{X_L} \\ \boldsymbol{Y_L} \\ \boldsymbol{Z_L} \end{bmatrix} \tag{2}$$

$\boldsymbol{v}$ and $\boldsymbol{r}$ are the instantaneous velocity and position vectors respectively.

3. Linearized model

The dynamic model for LEO's motion is deduced in terms of spherical coordinates referenced to the NORF. The radius vector $\boldsymbol{r}$ connects the Earth's and LEO's CoM. Its unitary vector is represented by $\boldsymbol{e_r}$. The true anomaly ($\boldsymbol{\theta}$) has as unitary vector $\boldsymbol{e_\theta}$ and the declination in NORF ($\boldsymbol{\phi}$) has as unitary vector $\boldsymbol{e_\phi}$. From the above definitions, it can be demonstrated that spherical and cartesian coordinates in the NORF are related by the following expression:

$$\begin{bmatrix} \boldsymbol{e_r} \\ \boldsymbol{e_\theta} \\ \boldsymbol{e_\phi} \end{bmatrix} = \begin{bmatrix} \cos\phi\cos\theta & \cos\phi\sin\theta & \sin\phi \\ -\sin\theta & \cos\theta & 0 \\ -\sin\phi\cos\theta & -\sin\theta\sin\theta\cos\phi \end{bmatrix} \begin{bmatrix} \boldsymbol{e_{x\,N}} \\ \boldsymbol{e_{y\,N}} \\ \boldsymbol{e_{z\,N}} \end{bmatrix} \tag{3}$$

Since the direction of the cartesian unit vectors is fixed, the derivatives of the spherical unit vectors can be expressed as:

$$\begin{bmatrix} \dot{\boldsymbol{e}}_{\boldsymbol{r}} \\ \dot{\boldsymbol{e}}_{\boldsymbol{\theta}} \\ \dot{\boldsymbol{e}}_{\boldsymbol{\phi}} \end{bmatrix} = \begin{bmatrix} 0 & \dot\theta\cos\phi & \dot\phi \\ -\dot\theta\cos\phi & 0 & \dot\theta\sin\phi \\ -\dot\phi & -\dot\theta\sin\phi & 0 \end{bmatrix} \begin{bmatrix} \boldsymbol{e_r} \\ \boldsymbol{e_\theta} \\ \boldsymbol{e_\phi} \end{bmatrix} \tag{4}$$

Using (4), it can be deduced the linear velocity ($\dot{\boldsymbol{r}}$) and acceleration ($\ddot{\boldsymbol{r}}$) vectors in spherical coordinates:

$$\boldsymbol{r} = r\boldsymbol{e_r} \tag{5}$$

$$\dot{\boldsymbol{r}} = \dot r\boldsymbol{e_r} + r\dot{\boldsymbol{e}}_{\boldsymbol{r}} = \dot r\boldsymbol{e_r} + (r\dot\theta\cos\phi)\boldsymbol{e_\theta} + \dot\phi\boldsymbol{e_\phi} \tag{6}$$

$$\begin{aligned} \ddot{\boldsymbol{r}} &= \ddot r\boldsymbol{e_r} + \dot r\dot{\boldsymbol{e}}_{\boldsymbol{r}} + (\dot r\dot\theta\cos\phi + r\ddot\theta\cos\phi - r\dot\theta\dot\phi\sin\phi)\boldsymbol{e}_\theta + \\ &\quad r\dot\theta\cos\phi\dot{\boldsymbol{e}}_\theta + (\dot r\dot\theta + r\ddot\phi)\boldsymbol{e}_\phi + r\dot\phi\dot{\boldsymbol{e}}_{\boldsymbol{\phi}} \\ \ddot{\boldsymbol{r}} &= (\ddot r - r\dot\theta^2\cos^2\phi - r\dot\phi^2)\boldsymbol{e}_r + \\ &\quad (r\ddot\theta\cos\phi + 2\dot r\dot\theta\cos\phi - 2r\dot\theta\dot\phi\sin\phi)\boldsymbol{e}_\theta \\ &\quad +(r\ddot\phi + 2\dot r\dot\phi + r\dot\theta^2\sin\phi\cos\phi)\boldsymbol{e}_\phi \end{aligned} \tag{7}$$

Rearranging (7) in terms of the spherical acceleration components and using the Newton's gravitational law, it is obtained the following system of equations for a non-perturbed (Keplerian) orbit in spherical coordinates:

$$\ddot{r} - r\dot{\theta}^2\cos^2\phi - r\dot{\phi}^2 + \frac{\mu_\oplus}{r^2} = 0 \quad (8)$$

$$r\ddot{\theta}\cos\phi + 2\dot{r}\dot{\theta}\cos\phi - 2r\dot{\theta}\dot{\phi}\sin\phi = 0 \quad (9)$$

$$r\ddot{\phi} + 2\dot{r}\dot{\phi} + r\dot{\theta}^2\sin\phi\cos\phi = 0 \quad (10)$$

In order to deduce the complete dynamic description of the system, the force model (8)-(10) is complemented with the vector perturbation forces (d_i), the residual terms (zonal and tesseral harmonics) of the gravitational model (g_i), and the vector of control variables (u_i) to be applied by the propulsion subsystem:

$$\ddot{r} - r\dot{\theta}^2\cos^2\phi - r\dot{\phi}^2 + \frac{\mu_\oplus}{r^2} = \frac{d_r}{m} + g_r + \frac{u_r}{m} \quad (11)$$

$$r\ddot{\theta}\cos\phi + 2\dot{r}\dot{\theta}\cos\phi - 2r\dot{\theta}\dot{\phi}\sin\phi = \frac{d_\theta}{m} + g_\theta + \frac{u_\theta}{m} \quad (12)$$

$$r\ddot{\phi} + 2\dot{r}\dot{\phi} + r\dot{\theta}^2\sin\phi\cos\phi = \frac{d_\phi}{m} + g_\phi + \frac{u_\phi}{m} \quad (13)$$

Where, m represents the mass of the LEO. Selecting as state variables the three spherical coordinates and its derivates, it is defined the following non-linear model for the LEO's orbit dynamics:

$$\dot{r}(t) = v(t) \quad (14)$$

$$\dot{v}(t) = r(t)\omega_\theta^2(t)\cos^2\phi(t) + r(t)\omega_\phi^2(t) - \frac{\mu_\oplus}{r^2(t)} + \frac{d_r}{m} + g_r + \frac{u_r}{m} \quad (15)$$

$$\dot{\theta}(t) = \omega_\theta(t) \quad (16)$$

$$\dot{\omega}_\theta(t) = \frac{-2v(t)\omega_\theta(t)}{r(t)} + 2\omega_\theta(t)\omega_\phi(t)\tan\phi(t) + \frac{d_\theta}{mr(t)\cos\phi(t)} + \frac{g_\theta}{r(t)\cos\phi(t)} + \frac{u_\theta}{mr(t)\cos\phi(t)} \quad (17)$$

$$\dot{\phi}(t) = \omega_\phi(t) \quad (18)$$

$$\dot{\omega}_\phi(t) = \frac{-2v(t)\omega_\phi(t)}{r(t)} - \omega_\theta^2(t)\sin\phi(t)\cos\phi(t) + \frac{d_\phi}{mr(t)} + \frac{g_\phi}{r(t)} + \frac{u_\phi}{mr(t)} \quad (19)$$

An analysis of (11)-(13) and (14)-(19) reveals that a direct analytical solution is not viable due to the coupling of non-linear ordinary differential equations. Approximation techniques shall be used, taking into account that d_i, g_i and u_i are assumed to be external input signals. It is also evident, that the variable $\theta(t)$ does not appear in the dynamic model. This fact is of special importance for the definition of a nominal model, where a nominal value of $\theta(t)$ has not influence. The orbit of the GOCE is characterized for: a low eccentricity (< 0.005), a high inclination angle, a mean altitude (r_0) of $250km$ and a quasi constant angular velocity (ω_0) of $1.17mrad/s$ [1]. Considering these conditions as a nominal scenario and developing the corresponding linearization

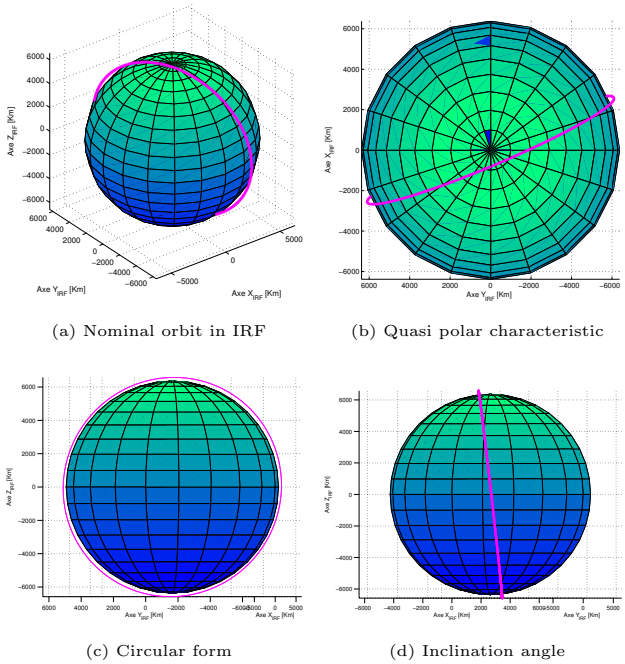

(a) Nominal orbit in IRF (b) Quasi polar characteristic

(c) Circular form (d) Inclination angle

Fig. 3. Simulation results evidencing nominal orbit characteristics

of (15), (17) and (19), the satellite's orbit dynamics can be approximated through the following linear model:

$$\begin{bmatrix} \dot{\hat{r}} \\ \dot{\hat{v}} \\ \dot{\hat{\theta}} \\ \dot{\hat{\omega}}_\theta \\ \dot{\hat{\phi}} \\ \dot{\hat{\omega}}_\phi \end{bmatrix} = \begin{bmatrix} 0 & 1 & 0 & 0 & 0 & 0 \\ 3\omega_o^2 & 0 & 0 & 2r_o\omega_o & 0 & 0 \\ 0 & 0 & 0 & 1 & 0 & 0 \\ 0 & -2\frac{\omega_o}{r_o} & 0 & 0 & 0 & 0 \\ 0 & 0 & 0 & 0 & 0 & 1 \\ 0 & 0 & 0 & 0 & -\omega_o^2 & 0 \end{bmatrix} \begin{bmatrix} \hat{r} \\ \hat{v} \\ \hat{\theta} \\ \hat{\omega}_\theta \\ \hat{\phi} \\ \hat{\omega}_\phi \end{bmatrix} + \begin{bmatrix} 0 & 0 & 0 \\ \frac{1}{m} & 0 & 0 \\ 0 & 0 & 0 \\ 0 & \frac{1}{r_o m} & 0 \\ 0 & 0 & 0 \\ 0 & 0 & \frac{1}{r_o m} \end{bmatrix} \begin{bmatrix} \hat{d}_r \\ \hat{d}_\theta \\ \hat{d}_\phi \end{bmatrix} + \begin{bmatrix} 0 & 0 & 0 \\ \frac{1}{m} & 0 & 0 \\ 0 & 0 & 0 \\ 0 & \frac{1}{r_o m} & 0 \\ 0 & 0 & 0 \\ 0 & 0 & \frac{1}{r_o m} \end{bmatrix} \begin{bmatrix} \hat{u}_r \\ \hat{u}_\theta \\ \hat{u}_\phi \end{bmatrix} \quad (20)$$

This linear model represents the incremental dynamics, due to exogenous perturbations, around a nominal circular orbit with constant radius (r_0) and constant angular velocity (ω_0). It is important to remark that residual gravitational terms are not included into the perturbations to be rejected, because the GOCE mission is oriented to measured such gravity anomalies. A detail analysis of (20), shows interesting characteristics of the linear approximation: first, the orbit plane dynamics and the NORF declination coordinate are decoupled. This means that if (20) is used for the controller synthesis, motion in the orbit plane can be considered separately from the out-of-plane dynamics. Also, it is evident that the polar angle of the orbit plane ($\hat{\theta}$), is not present in the dynamics described by (20), confirming its nature as cyclic variable. Based on the above conclusions, the linear approximation can be studied as three separate systems: a third order system (dynamics in the orbit plane), a second order system (the out of plane dynamics) and a first order

system (a cycle variable that not requires control). This is one of the most important results of the modelling approach followed, considering that a non-linear problem is adequately approximate, for a LEO with low eccentricity, into a linear decoupled plant.

4. Uncertainty modelling

In order to characterized the error introduced by the assumption of a circular nominal orbit, a comparative study is developed between this scenario and the numerical solution of the non-linear model described in (8)-(10). The conclusions demonstrate that error in the radial component is less than 1% while in the angular component is less than 9%. Thus, parametric uncertainty can be used in (20), considering the following parameter sets:

$$r_0 = \bar{r}_0(1 + 0.01\Delta_r) \text{ with } |\Delta_r| \leq 1 \quad (21)$$

$$\omega_0 = \bar{\omega}_0(1 + 0.09\Delta_\omega) \text{ with } |\Delta_\omega| \leq 1 \quad (22)$$

Other sources of uncertainty are the unmodeled dynamics of sensors (gradiometer) and actuators (thrusters), the effects of exogenous disturbance not characterized (see section 5) and the impact of noise in different channels of the controlled system (measurements, control signals). Only recent works [2] supply base information to attempt a frequency quantification that describes the effect of the mentioned sources of uncertainty, specially in the Measurement Bandwidth (MBW). The techniques for gravity field determination on the GOCE mission are based on Precise Orbit Determination (GPS /GLONASS orbit monitoring to *cm*-precision) and Satellite Gravity Gradiometry. The intersection of both techniques leads to the definition of the mentioned Measurement Bandwidth (MBW) between $5mHz$ and $0.1Hz$ [1]. In order to maintain conservative specifications, the effects of parametric and unmodeled dynamics (spectrally estimated) are lumped through an Input Multiplicative Uncertainty Model (IMUM), that generates the following set of plants for which the synthesized controller shall guarantee stability and performance requirements:

$$\hat{G}(s) = \hat{G}_{nom}(1 + \Delta(s)) \text{ with } |\Delta(j\omega)| \leq 0.68 \ \forall\omega \quad (23)$$

5. Analysis of exogenous disturbances and control specifications

As stated before, the GOCE mission requires an important attenuation of non-gravitational disturbances (mainly drag forces) in the MBW. In order to deduced the quantitative value of this performance specification, a characterization of the Power Spectral Density (PSD) of the along track atmospheric drag forces is carried out through a comparative study between non-parametric methods (periodogram, Welch, multitaper), parametric methods (Yulear, Burg) and subspace methods (MUSIC, eigenvector). Particularly interest is concentrated into the MBW where the control system has the most stringent work conditions. First results are developed analyzing the drag forces in the LORF (see Fig. 5). Through the PSD estimation with non-parametric methods (multitaper with time-bandwidth product equal to 4), it is

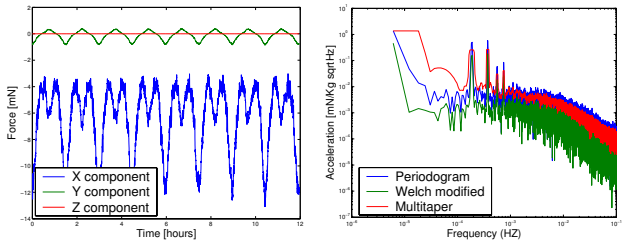

(a)Atmospheric drag time series (courtesy of Alenia Spazio)

(b)Non-Parametric methods

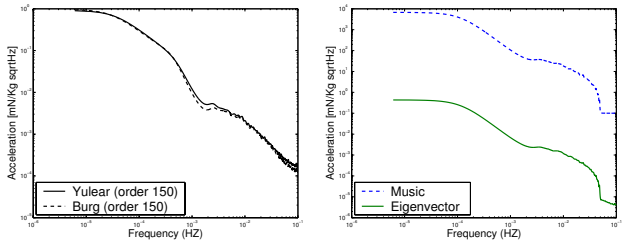

(c)Parametric methods

(d)Subspace methods

Fig. 4. Spectral analysis of atmospheric drag

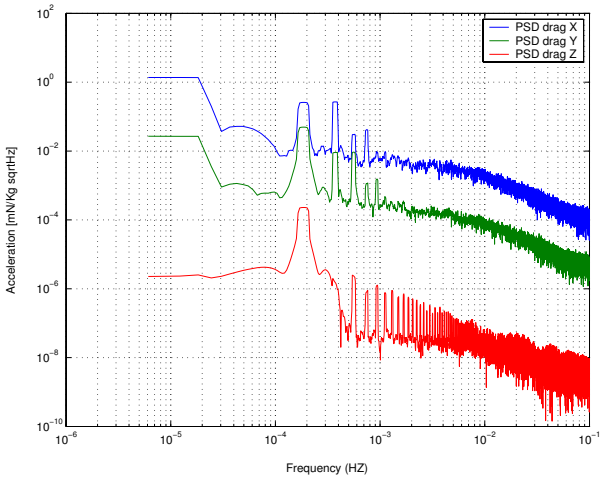

Fig. 5. PSD of drag accelerations in the LORF

evident that most part of the impact of atmospheric drag is concentrated at low frequencies and specially, at the fundamental and second harmonic of the nominal angular velocity ω_0 (fact that is consistent with the eccentric characteristics of the orbit). Using parametric methods (Yulear with order 150) and subspace methods (eigenvector with order 50) for PSD estimation, the worst case of drag spectrum is obtained. Using this results and taking into account that atmospheric drag increase its effect at lower distance from Earth's surface, emerge an important constraint for the problem: if a circular orbit (with radius equivalent to the distance at perigee) is to be considered as nominal case, then the higher magnitude of drag forces shall be used for determining the attenuation specifications. Using the respective transformation matrices, the worst case of atmospheric drag and the maximum allowable disturbance level [2] are rotated to the NORF and finally analyzed into this reference frame (see fig. 6).

Comparing the atmospheric drag PSD with the maximum allowable disturbance level in the NORF, the quantitative

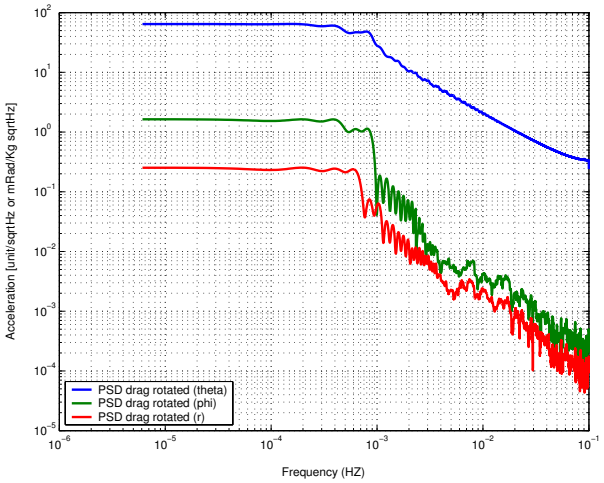

Fig. 6. PSD of drag accelerations in the NORF

attenuation levels are deduced as a function of frequency. In order to guarantee conservative results, a minimum attenuation of $35dB$ from D.C to $0.1Hz$ is assumed as main performance specification for the orbit plane controller. More relaxed specifications can be defined for the out of plane dynamics, due to the fact that worst drag effect in this direction is under the maximum allowable disturbance level (theoretically, a controller is not required). It is important to remark that a deeper analytical cross check between the transformations made from LORF to NORF and the techniques for gravity field determination on the GOCE mission remains to be assessed.

6. control synthesis

The approach followed during the plant modelling define a decentralized architecture of the control system. In fact, one controller is related with the orbit plane dynamics, which are characterized by a two input two output (TITO) model. The output variables to be considered for this model are the incremental accelerations in the radial and tangent direction. It is important to remark that such measures can be deduced from GOCE sensors, with the subsequent transformation to the NORF. However, the role of such techniques requires a deeper formalization and treatment. The second controller is associated with the out of plane dynamics, which are characterized by a SISO model, considering the incremental elevation angle acceleration as output. Same considerations made for orbit plane acceleration measures applied here. For the TITO and SISO systems described before, the objective is to find a controller $K(s)$ that guarantees stability and the fulfillment of the performance requirements (as deduced in section 5) in presence of input multiplicative uncertainty (with weighting functions as indicated in (23)). The proposed approach for the synthesis of the orbit controller starts with a scaling of plant outputs and inputs (time and amplitude un-dimensionalization), in order to improve the numerical conditioning of the design problem. Then, a controllability (stabilizability) and observability (detectability) analysis is developed, revealing an interesting conclusion in terms of the effect of the control signals into the system dynamics. Specifically, it is explicit a complete controllability of the orbit plane dynamics from the tangent component (u_θ). This is an important aspect to be assessed in a later treatment of balanced thrusters function and in the optimization of the satellite's propulsion subsystem. The robust control problem is then formulated in the frame work of modern $H\infty$ synthesis theories for Singular Value (SV) shaping. The weighting functions of the augmented plant are adjusted to find an adequate trade-off between input multiplicative model uncertainty ($|\Delta(j\omega)|$), disturbance attenuation and penalty in the control signal (Figs. 7 and 8). It is important to remark

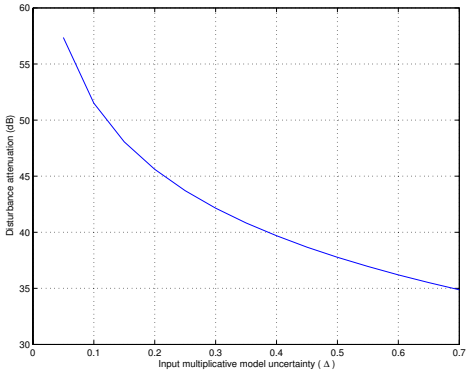

Fig. 7. Input multiplicative model uncertainty vs. disturbance attenuation

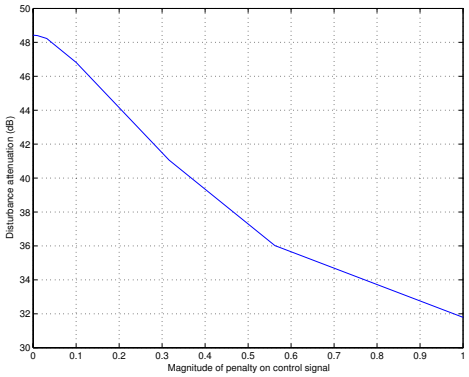

Fig. 8. Penalty in the control signal vs. disturbance attenuation

that the $H\infty$ controller is obtained through a Linear Matrix Inequality (LMI) approach, due to the undamped dynamics that characterize the linear approximation (this situation makes unfeasible to find a solution with classical matlab algorithms as in [7]). Also, the LMI approach offers a more flexible frame for $H\infty$ synthesis because requires only two main assumptions in the augmented model [8]: one, the pairs A, B_2 and A, C_2 shall be stabilizable and detectable respectively; second, D_{22} shall be equal to zero. The verification of the robustness characteristics are made through the Singular Value Decomposition of the transfer matrix from the disturbances to the objectives in the controlled system (T_{uy}), whose graphical results (Fig. 9) confirm that $\|T_{uy}\|_\infty \leq 1$ for all frequencies. Also, in Fig. 10 is presented the maximum singular values of the transfer matrix that relates the dis-

turbances to the measured variables, confirming that they are under the imposed bound (performance weight). The graphics presented are referred to the scaled system (hence, $1rad/s$ is equivalent to $1.17mrad/s$ in the original system).

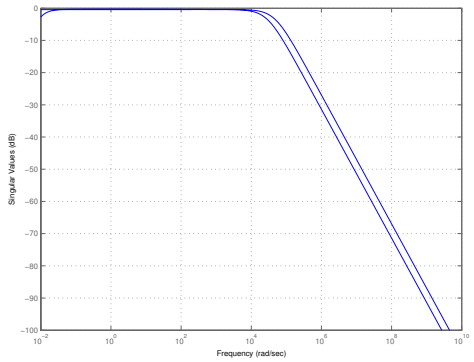

Fig. 9. Max. singular values of cost function T_{uy}

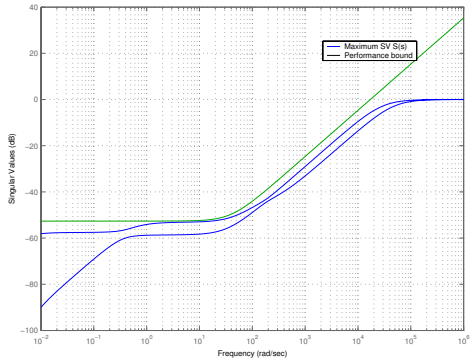

Fig. 10. Singular values of sensitivity function

7. Simulation results

The synthesized controller was tested using the scaled model that integrates the nominal dynamics and the orbit relative motion as approximated in (20). In Fig. 11 is presented the output response in the tangent component ($\hat{\boldsymbol{\theta}}$) for the worst case scenario: a sinusoidal force drag signal (normalized in amplitude and in frequency) with frequency equivalent to the nominal ω_0 (here normalized to $1rad/s$). The maximum amplitude of the incremental radial acceleration, for this case, is around $2e-3$, confirming a disturbance attenuation of approximately $54dB$.

8. Conclusions

In this paper is proposed a modern approach for the attenuation of the atmosphere drag effects into the orbit trajectory of a LEO. The main contributions are related with the definition of a linear decoupled plant, a detail frequency characterization of the drag disturbances and a simplified approach to $H\infty$ robust control synthesis based on an LMI approach. The resulting controller stabilizes the plant and maintain drag attenuation specifications in presence of input multiplicative uncertainty with a weighting function equivalent to $|\Delta(j\omega)| \leq 0.68\ \forall\omega$.

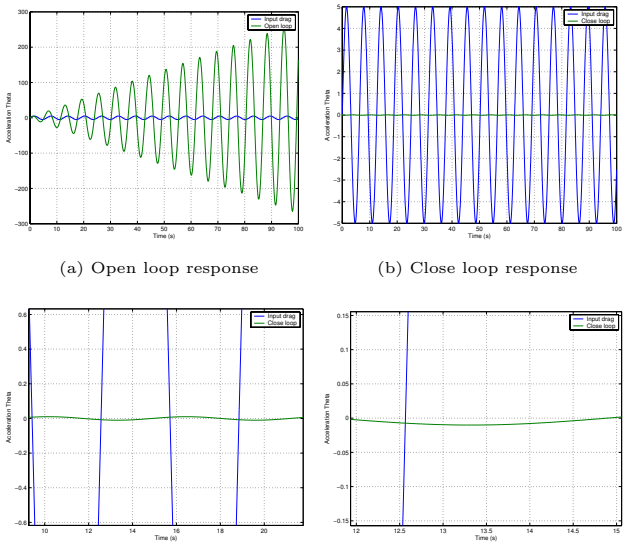

(a) Open loop response (b) Close loop response

(c) Zoom of close loop response (d) Output maximum value

Fig. 11. Time response to a sinusoidal input

Acknowledgments

The authors would like to thank Alenia Spazio (Turin, Italy), main contractor of the GOCE satellite, for the information supplied for the development of this work.

References

[1] ESA, *GOCE mission requirements document*, ESA Publications Division, 2000

[2] E. Canuto, B. Bona, M. Indri, and G. Calafiore, "Drag free control for the European satellite GOCE. part I: modeling," in *Procedings of the 41st IEEE conference on Decision and Control Conference*, Las Vegas, USA, December 2002, pp. 1269–1274.

[3] E. Canuto, B. Bona, M. Indri, and G. Calafiore, "Drag free control for the European satellite GOCE. part II: digital control," in *Procedings of the 41st IEEE conference on Decision and Control Conference*, Las Vegas, USA, December 2002, pp. 4072–4077.

[4] O. Montenbruck, and E. Gill, *Satellite orbits: models, methods and applications*, Springer, Berlin, 2000.

[5] S. Boyd, L. El Ghaoui, E. Feron, and V. Balakrishnan, *Linear matrix inequalities in systems and control theory*, SIAM books, Philadelphia, 1994.

[6] G. E. Dullerud and F. Paganini, *A course in robust control theory : a convex approach*. New York: Springer, 2000.

[7] R. Chiang and M. Safonov, *Robust control toolbox*, 2nd ed., Mathworks, Natick, MA, 1997.

[8] P. Gahinet, and P. Apkarian, "A linear matrix inequality approach to $H\infty$ control," *International Journal of robust and nonlinear control*, vol. 4, pp. 421–448, 1994.

[9] M. Sidi, *Spacecraft dynamics and control*, Cambrigge University Press, New York, 1997.

[10] P. Gahinet, A. Nemirovski, A. J. Laub, and M. Chilali, *LMI control toolbox*, Mathworks, Natick, MA, 1st edition, 1995.